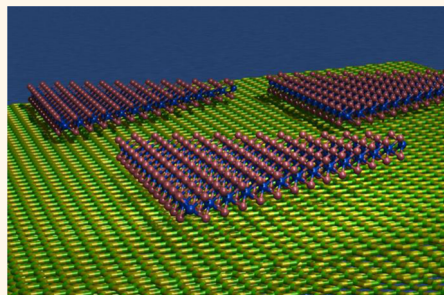


All Chemical Vapor Deposition Growth of MoS₂:h-BN Vertical van der Waals Heterostructures

Shanshan Wang, Xiaochen Wang, and Jamie H. Warner*

Department of Materials, University of Oxford, Parks Road, Oxford OX1 3PH, United Kingdom

ABSTRACT Vertical van der Waals heterostructures are formed when different 2D crystals are stacked on top of each other. Improved optical properties arise in semiconducting transition metal dichalcogenide (TMD) 2D materials, such as MoS₂, when they are stacked onto the insulating 2D hexagonal boron nitride (h-BN). Most work to date has required mechanical exfoliation of at least one of the TMDs or h-BN materials to form these semiconductor:insulator structures. Here, we report a direct all-CVD process for the fabrication of high-quality monolayer MoS₂:h-BN vertical heterostructured films with isolated MoS₂ domains distributed across 1 cm. This is enabled by the use of few-layer h-BN films that are more robust against decomposition than monolayer h-BN during the MoS₂ growth process. The MoS₂ domains exhibit different growth dynamics on the h-BN surfaces compared to bare SiO₂, confirming that there is strong interaction between the MoS₂ and underlying h-BN. Raman and photoluminescence spectroscopies of CVD-grown MoS₂ are compared to transferred MoS₂ on both types of substrates, and our results show directly grown MoS₂ on h-BN films have smaller lattice strain, lower doping level, cleaner and sharper interfaces, and high-quality interlayer contact.



KEYWORDS: vertical heterostructures · MoS₂ · h-BN · all-CVD growth · optical properties

Rapid progress in the research of two-dimensional (2D) atomic crystals, such as graphene, monolayer and multilayer hexagonal boron nitride (h-BN), and transition metal dichalcogenides (TMDs), has extended to the fabrication of vertical heterostructures with different types of 2D crystals stacking on top of each other. The flexible and transparent heterostructures compiled by van der Waals stacking of various 2D materials produce novel heterojunctions that have great potential in electronic and optoelectronic applications.^{1–5} The layer-by-layer heterostructures were first created by stacking different types of materials through sequential mechanical transfer techniques.¹ However, this method is complicated with several disadvantages, such as contamination at the interface, the low quality of interlayer contact, the significant requirements on the position control for different 2D crystals stacking on top of each other, and the lack of future scalable production for large-area coverage.^{1,6–8} The direct growth of vertical layered heterostructures *via* chemical vapor deposition (CVD) is much

more promising in terms of scalability. Recent advances have demonstrated that vertical heterostructures, such as graphene/h-BN,⁹ MoS₂/graphene,¹⁰ MoSe₂/graphene,¹¹ MoS₂/h-BN,¹² WS₂/h-BN,¹³ MX₂/SnS₂ (M = Mo, W; X = S, Se),¹⁴ and WS₂/MoS₂,⁸ can be grown by CVD. Growing 2D materials on h-BN exploits the advantage that h-BN has an atomically flat surface without dangling bonds and charged impurities, as well as being chemically inert, which leads to improvements in the device performance and optical properties.^{15,16} However, for CVD-grown TMD heterostructures on h-BN substrates, there still exist challenges in utilizing CVD-grown h-BN rather than mechanically exfoliated h-BN.

The h-BN obtained by mechanical exfoliation has a small flake size, and therefore, it is not possible to create large millimeter or centimeter scale heterostructured materials that could be used in large-area optoelectronics like solar cells, photodetectors, and 2D imaging arrays. Prior work on the direct growth of MoS₂/h-BN heterostructures by CVD used organic seeding promoters to

* Address correspondence to jamie.warner@materials.ox.ac.uk.

Received for review January 29, 2015 and accepted April 14, 2015.

Published online April 20, 2015
10.1021/acsnano.5b00655

© 2015 American Chemical Society

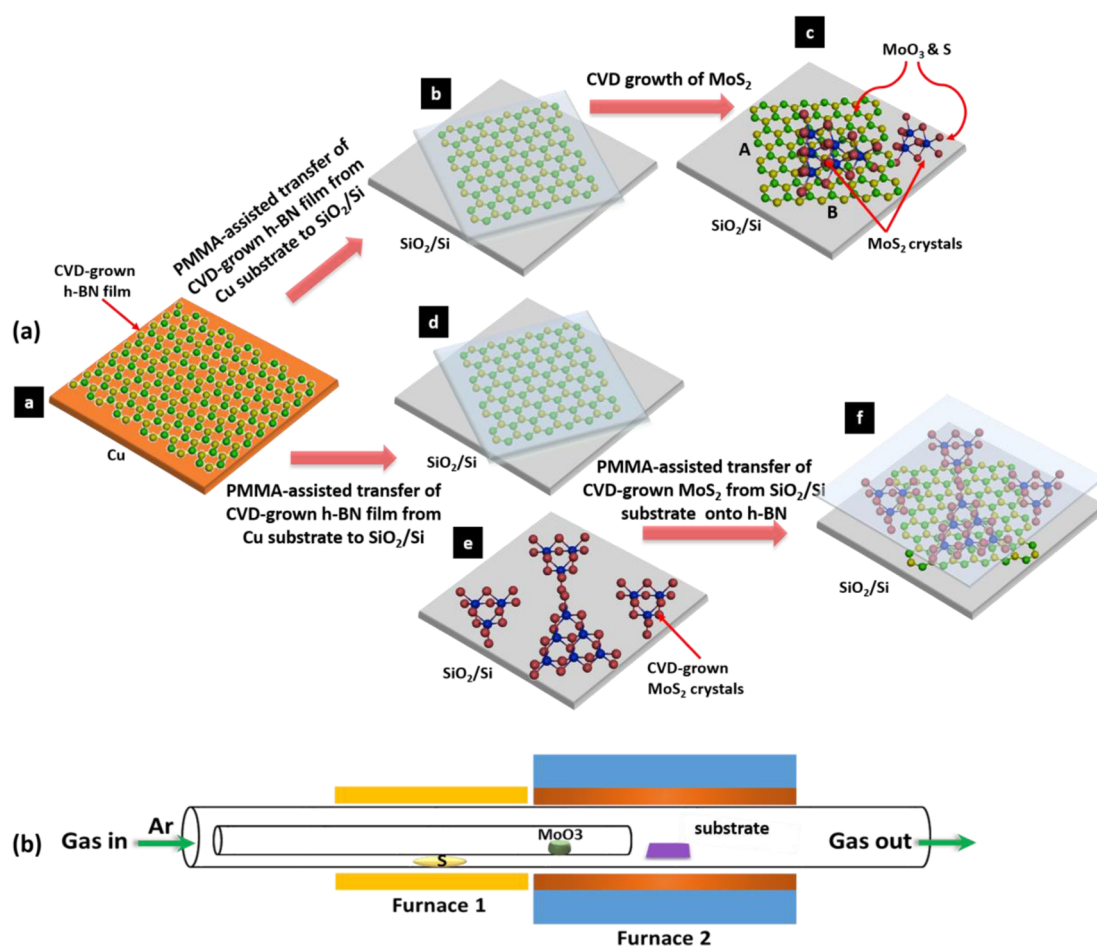


Figure 1. (a) Schematic illustration of two fabrication processes of MoS₂/h-BN heterostructures. The first method is initially transferring the CVD-grown h-BN film from a copper foil to the center of a SiO₂/Si chip, leaving four corners of the substrate to be bare SiO₂ surface. This substrate is then loaded face-up into the CVD system to grow MoS₂ on it. The MoS₂ domains will cover both h-BN and SiO₂ areas. The second approach is through a two-step PMMA-assisted transfer process. The CVD-grown h-BN film was still first transferred onto the center of a SiO₂/Si chip surface, followed by stacking another layer of CVD-grown MoS₂ domains on the whole substrate surface, obtaining transferred MoS₂ domains on h-BN in the central area and on SiO₂ at four corners. Two of the transfer boundaries of the h-BN film on the SiO₂ surface in the first fabrication method are labeled by the letters of A and B, respectively. (b) Schematic illustration of the CVD system for MoS₂ growth.

help nucleate the MoS₂ on exfoliated h-BN,¹² which might remain at the interface between MoS₂ and h-BN after growth and have some influence on the properties of these heterostructures. Ideally, a scalable approach for directly growing seed-free MoS₂ on CVD-grown h-BN is needed.

There are several challenges that must be overcome in order to successfully grow a TMD on h-BN by an all-CVD approach. First, the h-BN grown on Cu by CVD needs to be transferred to an alternative substrate because the S will react the Cu. The transfer of CVD-grown h-BN films from Cu to TMD growth-compatible substrates like Si:SiO₂ or sapphire must be clean, with the polymer scaffold used for transfer removed to leave an exposed h-BN surface for direct growth of TMDs. The growth temperature should not be too high because this will increase the decomposition of the h-BN film before the TMD has been grown. This suggests that the lower growth temperature of MoS₂ compared to that of WS₂ is preferred. The process should be hydrogen-free,

as the introduction of H₂ gas at high temperature will decompose the h-BN film. Residual oxygen in the CVD system and oxygen species available from the metal-oxide precursor commonly used to grow TMDs are likely to also etch the h-BN during the CVD growth of TMDs.

RESULTS AND DISCUSSION

Two-dimensional MoS₂ crystals are grown on the substrate of CVD-grown h-BN film under atmospheric pressure using MoO₃ (molybdenum trioxide) and sulfur powder as precursors. When we attempted to grow MoS₂ on monolayer h-BN films, we found that the h-BN had been substantially decomposed by the growth process and led to poor samples. Alternatively, we found that using few-layer h-BN films (2–4 layers) was ideal because the films were more robust against degradation during the growth and enabled successful deposition of precursor and ultimately the growth of MoS₂ domains on a continuous few-layer h-BN film. Steps of a, b, and c in Figure 1a present the fabrication

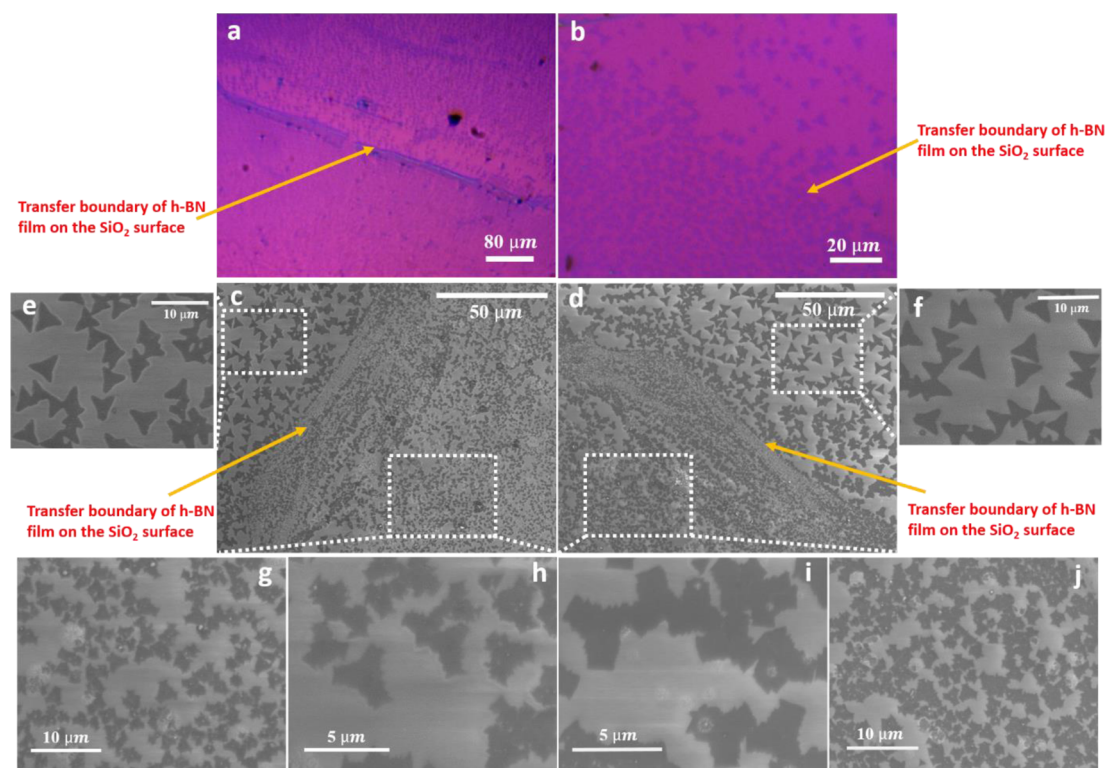


Figure 2. (a,b) Optical microscopy images of the edge region of the h-BN film on the SiO₂ surface, showing MoS₂ crystals grown by CVD both on and off the h-BN film. (c,d) SEM images of CVD-grown MoS₂ crystals around the edge region of the h-BN film on the SiO₂ surface marked by letters of A and B, respectively, in step c of Figure 1a. (e,f) Zoomed-in SEM images of MoS₂ crystals grown on the SiO₂ in the region of white boxes shown in panels c and d, respectively. (g–j) Zoomed-in SEM images of MoS₂ crystals grown on the h-BN film in the region of white boxes shown in panels c and d, respectively.

process of the MoS₂/h-BN vertical heterostructures by CVD. The few-layer h-BN film was initially grown on the Cu substrate by CVD using an ammonia borane precursor and then transferred onto the central area of a bare SiO₂/Si chip by a poly(methyl methacrylate) (PMMA)-assisted method, leaving four corners of the substrate as bare SiO₂ surfaces. The PMMA was removed by acetone to leave a clean h-BN. The substrate with h-BN was subsequently loaded into the CVD system designed for the growth of 2D MoS₂ on the top of both h-BN film and SiO₂. In order to compare the differences between directly growing MoS₂ on h-BN by the CVD method with those fabricated by a transfer process, as seen in steps a, d, e, and f in Figure 1a, we also did MoS₂/h-BN heterostructures *via* a two-step PMMA-assisted transfer approach. This involved replacing the direct CVD synthesis of MoS₂ (step c) with another transfer process of the CVD-grown 2D MoS₂ crystals from the original Si chip to a new SiO₂/Si substrate having h-BN film covered in the center and SiO₂ exposed at four corners (steps e and f). For the CVD system of MoS₂ growth, as depicted in Figure 2b, two separated furnaces were used to realize better temperature control on both precursors and the substrate. Six hundred milligrams of sulfur powder and the substrate were put in the center of furnaces 1 and 2, respectively, where the temperature can be independently controlled. MoO₃ powder was loaded in

the upstream of the second furnace, where the heating temperature can be adjusted by changing the distance between MoO₃ and the furnace center. It is noteworthy that, instead of placing two precursors in the same tube, we put 20 mg of MoO₃ powder in a separated mini-tube (diameter 1 cm) inside the outer 1 in. tube, with its gas inlet loading far before the sulfur location.¹⁷ This is to avoid any cross-contamination between sulfur and MoO₃ powder when supplying precursors into the growth area because sulfur vapor can react with solid-state MoO₃ at its evaporation temperature (~300 °C) in our experiment and decrease its amount, leading to the attenuation of MoO₃ evaporation rate and thus resulting in an unstable precursor supply in the vapor phase. The substrate, having CVD-grown h-BN films pretransferred onto the central area, was placed horizontally in the center of the second furnace, which enables us to compare the 2D MoS₂ growth on different substrates. Typical growth temperatures used for sulfur, MoO₃, and the substrate are ~180, ~300, and ~800 °C, respectively. Sulfur powder was preheated before increasing the temperature of MoO₃ to ensure the sufficient supply of sulfur vapor in the growth system. The detailed growth recipe and a brief introduction about the “pulse style” precursor supply mode used in our experiment are provided in the Supporting Information. This simple, scalable CVD growth approach can realize the direct fabrication of large-area

MoS₂/h-BN heterostructures with a clean interface and good interlayer contact, which is advantageous over a mechanical transfer method.

Figure 2a,b shows optical microscope (OM) images around the transfer boundary of h-BN on SiO₂, showing that 2D MoS₂ growth occurs over a large area. The homogeneous color contrast of MoS₂ domains indicates the thickness uniformity. The 2D MoS₂ crystals grown on the h-BN film exhibit a pronounced higher nucleation density and smaller domain size, compared to those grown on the SiO₂, which may result from the higher roughness of transferred h-BN film on SiO₂ (Figure S1c of the Supporting Information). The small optical contrast from the h-BN film on SiO₂ can be attributed to its negligible opacity in the visible spectrum arising from its large band gap (>5 eV), making it hard to be detected.¹⁸ However, the existence of h-BN under 2D MoS₂ has been confirmed by Raman spectroscopy, which will be discussed later. The SEM images (Figure 2c–j) display more detailed information, such as the variations of MoS₂ crystal morphology on different substrates. It can be seen that MoS₂ crystals grown on SiO₂ are not exact triangles with sharp edges as normally observed, but rather, they are three-pointed star-shaped with an average domain size of ~5 μm. For those grown on h-BN, the crystal shape transforms to truncated three-point stars with a flake size decrease to ~3 μm. We interpret the formation of three-point star-shaped instead of triangular domains of MoS₂ on SiO₂ to the ultralow Mo:S ratio of precursors absorbed on the substrate and attribute the crystal shape and size difference between MoS₂ on h-BN and on SiO₂ to the growth rate and time variations arising from different interactions between precursor species and two types of substrate surfaces.¹⁹

Raman spectroscopy is a very useful technique to determine the layer number of MoS₂ by measuring the frequency difference between two characteristic vibration modes, E_{2g}¹ and A_{1g}.^{20,21} The E_{2g}¹ mode represents the in-plane vibration of molybdenum and sulfur atoms, while the A_{1g} mode is related to the out-of-plane vibration of sulfur atoms.²¹ Figure 3a shows the Raman spectra of the direct-grown MoS₂ on CVD-grown h-BN film and on SiO₂, respectively, with an excitation wavelength of 532 nm. The fitting results show that, for MoS₂ grown on h-BN, these two modes are centered at ~380.6 and 401.2 cm⁻¹, respectively, while those MoS₂ domains grown on SiO₂ have two vibration modes located at ~382.4 and ~402.9 cm⁻¹, respectively, both giving a frequency difference of ~20.5 cm⁻¹. This is compatible with the CVD-grown monolayer MoS₂ in previous works.^{12,22,23} The inset of Figure 3a is the measured characteristic Raman peak of CVD-grown h-BN under MoS₂ domains, which is located at ~1372 cm⁻¹, confirming the existence of the h-BN film after experiencing the growth process of

MoS₂. A line scan was also carried out, measuring the Raman spectrum point-by-point for the characteristic h-BN vibration mode across a transfer boundary of h-BN film on SiO₂, marked by the dashed black line in Figure 3b. Figure 3c shows a plot of the integrated h-BN Raman peak as a function of distance, and it rapidly disappears in the central region. It confirms that this region is the edge of the transferred h-BN film on SiO₂, and Figure 3d,e shows examination of the boundary region.

We also observed peak location variations of both modes when MoS₂ was grown on different substrates. In Figure 3a, compared to the Raman spectra of MoS₂ grown on SiO₂, a pronounced phonon mode stiffening reflected by the blue shift of both E_{2g}¹ and A_{1g} peaks can be observed for MoS₂ grown on h-BN. The variations are measured to be ~1.8 and 1.7 cm⁻¹ for E_{2g}¹ and A_{1g} modes, respectively. We also performed Raman mappings around the region of a transfer boundary, where half of the mapping area had the monolayer MoS₂ grown on the h-BN film and another half had MoS₂ on SiO₂ (Figure 3b). By plotting the 2D spatial variation of the magnitude of E_{2g}¹ and A_{1g} peak frequency separately (Figure 3d,e), it can be found that the frequency difference for these two characteristic vibration modes, depending on the growth substrate, is ubiquitously observed on the sample. Furthermore, we also investigated the substrate effect on transferred CVD-grown MoS₂ domains on these two types of materials, h-BN film and SiO₂, via a two-step PMMA-assisted transfer method (steps a, d, e, and f in Figure 1a). It was found that the MoS₂ on h-BN and on SiO₂ had the E_{2g}¹ peak centered at almost the same wavenumber, while the A_{1g} mode of MoS₂ on h-BN appeared as a slight blue shift in a value of ~0.7 cm⁻¹, compared to that of MoS₂ on SiO₂ (Figure 3f). This phenomenon can also be commonly observed on the sample by comparing the Raman mapping of frequencies for these two characteristic modes of MoS₂ on h-BN and on SiO₂, respectively (Figure 3g–j). The inset of Figure 3g shows the characteristic Raman vibration mode of the h-BN film lying underneath the transferred MoS₂ domains, which is measured to be at ~1368 cm⁻¹.

In addition to distinguishing the number of layers, Raman spectra can also be utilized to investigate other effects such as lattice strain, doping levels, and the van der Waals interaction at the interface for 2D crystals.^{24–30} The in-plane Raman mode, E_{2g}¹, is sensitive to the built-in strain of 2D MoS₂,^{25–27,29} and therefore, the E_{2g}¹ peak position variation of ~1.8 cm⁻¹ observed in Figure 3a can be attributed to the different strain effect in monolayer MoS₂ grown on h-BN and on SiO₂. In order to determine the MoS₂ lattice strain on these two types of substrates, we used the same growth method to produce MoS₂ on a bare SiO₂/Si substrate followed by measuring its Raman spectra and then transferred these MoS₂ domains onto

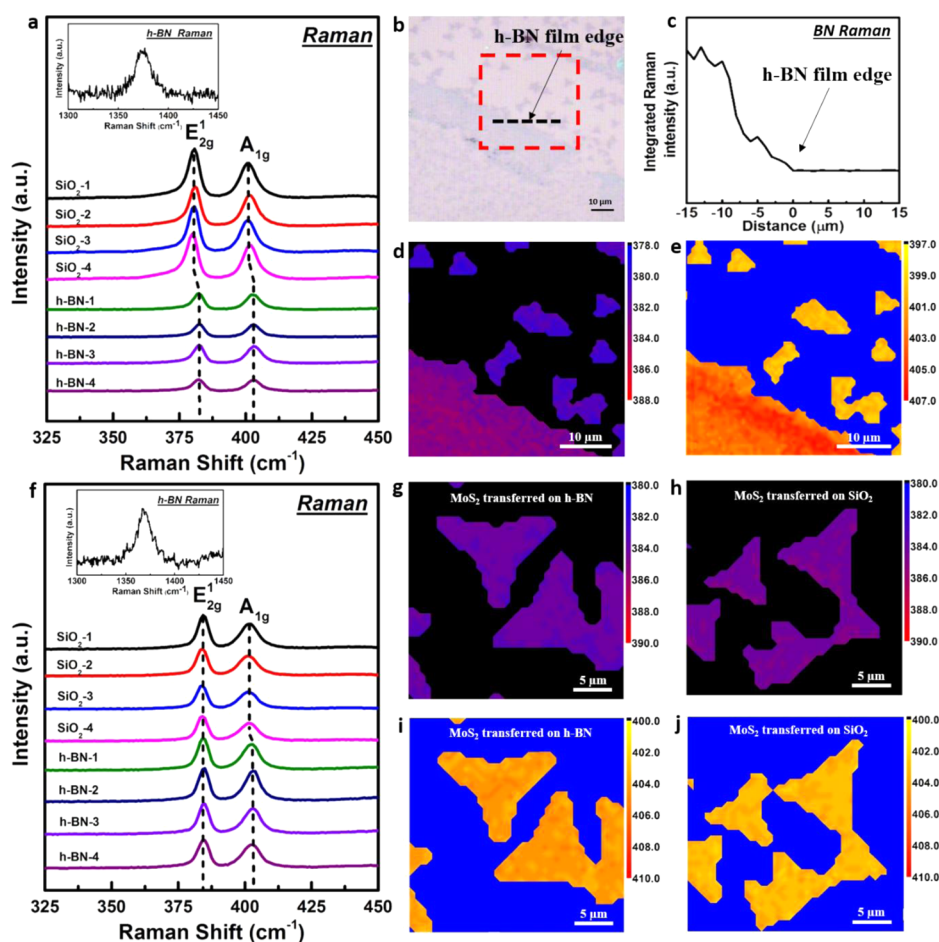


Figure 3. (a) Raman spectra collected from eight different MoS₂ domains grown on two types of substrates, four of which are grown on the SiO₂ surface and another four are grown on the h-BN film. The inset shows the Raman spectra measured from the h-BN film under the directly grown MoS₂ crystals. (b) Optical image showing the MoS₂ crystal growth around the region of the transferred h-BN film edge. (c) Plot of the integrated h-BN Raman peak intensity as a function of distance, which was measured across the edge of the h-BN film, marked by a black dashed line in panel b. The point on the curve which is indicated by a black arrow corresponds to the location of the h-BN film edge in panel b, as the integrated h-BN Raman peak disappears from this point. (d,e) Raman maps of direct-grown MoS₂ domains on different substrates, plotting the spatial variation of the peak position for E_{2g}¹ and A_{1g} modes, respectively, in the area of the red box marked in panel b, where the top right region has the substrate of SiO₂ and the left bottom area has the substrate of h-BN. (f) Raman spectra collected from eight different MoS₂ domains transferred on two types of substrates, four of which are transferred on the SiO₂ surface and another four are transferred on the h-BN film. The inset shows the Raman spectra measured from the h-BN film under the transferred MoS₂ crystals. (g–j) Raman maps of the peak position for E_{2g}¹ and A_{1g} modes of transferred MoS₂ domains on different substrates, h-BN and SiO₂.

another SiO₂/Si substrate and measured the Raman spectra again. The transfer process is aimed at releasing the potential strain that exists in the direct-grown MoS₂ crystals. It was found that the E_{2g}¹ mode of transferred MoS₂ crystals showed a blue shift of 1.7–2.0 cm⁻¹, compared to the direct-grown ones on SiO₂, while the A_{1g} peak position remained unchanged (Figure S4 of Supporting Information). Given that the Gruneisen parameter of the E_{2g}¹ mode is 0.54,³¹ we determined that the monolayer MoS₂ crystals grown on SiO₂ suffered a biaxial lattice tensile strain of ~0.45%, in agreement with the previous reports on CVD-grown monolayer MoS₂ on the same substrate.²⁵ Considering that the monolayer MoS₂ grown on h-BN has a ~1.8 cm⁻¹ blue shift of the E_{2g}¹ mode, which is quite similar to the frequency variation (1.7–2.0 cm⁻¹)

between the strain-free transferred MoS₂ and the direct-grown MoS₂ on SiO₂, it indicates that using the CVD-grown h-BN film as a substrate can lead to a much smaller lattice strain in monolayer MoS₂ grown above, which may arise from the weak van der Waals force at the interface of MoS₂/h-BN heterostructures, making the lattice strain easier to release. This conclusion is further supported by the negligible frequency difference of the E_{2g}¹ mode between transferred monolayer MoS₂ located on h-BN and on SiO₂, indicating that the E_{2g}¹ mode is barely affected by other factors, such as substrate materials, doping levels, interlayer contact, etc., except for the built-in strain. In terms of the A_{1g} mode, which is associated with the doping level, a stiffening of it at a value of ~1.7 cm⁻¹ for MoS₂ grown on h-BN film, compared with that on SiO₂, can be

attributed to the reduced electron density in monolayer MoS₂.^{32,33} Compared with SiO₂, h-BN is known to have a much lower degree of charged impurities, which can decrease the doping level of the above 2D MoS₂ because there will be less charge transfer from the substrate to MoS₂ through the interface, consistent with recent studies.^{34–36} The A_{1g} peak frequency difference between MoS₂ on h-BN and on SiO₂ drastically decreases from ~ 1.7 to ~ 0.7 cm⁻¹ when this contact mode is realized by the transfer process instead of direct growth. As aforementioned, there is no change on the A_{1g} peak position between the direct-grown and the transferred monolayer MoS₂ on SiO₂/Si. This means that, through the transfer process, the blue shift magnitude of the A_{1g} mode for MoS₂ on h-BN is obviously reduced. This could result from two reasons: one is the contamination from different kinds of solvents used during transfer, which spoil the clean interface and increase the doping effect;³³ another possible reason is the lower quality of an interlayer interaction between monolayer MoS₂ and the h-BN film underneath, which may arise from the higher surface roughness of the CVD-grown h-BN film transferred on SiO₂/Si compared to that on the bare SiO₂/Si surface.²⁶

However, as the laser-induced thermal effect can change the anharmonicity in the lattice potential energy of MoS₂, having an influence on both E_{2g}¹ and A_{1g} modes,^{26,37,38} one may argue that, in our experiment, the shift could also be produced by a laser-induced temperature contribution. In order to exclude any thermal effects, we set all experimental conditions used in each Raman measurement to be constant, so that the thermal effect would be approximately the same for different samples. Furthermore, we did a comparison experiment by decreasing the acquisition time from 2 to 0.5 s accompanied by a reduction on the number of spectra averaged for signal-to-noise enhancement from 2 to 1, and it was found that there was no obvious shift on the position of both E_{2g}¹ and A_{1g} peaks (Figure S5 of Supporting Information), which indicates that the laser-induced thermal perturbation in our experiment can be ignored.

The peak intensity as well as the intensity ratio between A_{1g} and E_{2g}¹ also shows slight differences for MoS₂ on different substrates. For transferred samples, the Raman intensity for both vibration modes of MoS₂ on h-BN appears stronger with a slightly higher intensity ratio of A_{1g}/E_{2g}¹ compared to that of MoS₂ on SiO₂ (Figure 3f). This could arise from the substrate-induced interference effects, as the absorption and the emission intensities can be strongly modulated by the interference within different types of substrates.²⁴ However, for the direct-grown MoS₂ on BN, even though the A_{1g}/E_{2g}¹ intensity ratio is still higher than that of the direct-grown MoS₂ on SiO₂, in agreement with the phenomenon observed in the transferred samples, the intensities of both characteristic modes

decrease drastically (Figure 3a). This could possibly be due to two reasons. One is the smaller MoS₂ domain size, which makes the precise focus of laser spots onto MoS₂ crystals under an optical microscope more difficult. The other reason is the higher roughness of monolayer MoS₂ domains grown on h-BN film because the contact quality between the direct-grown MoS₂ and h-BN film is higher than that of the transferred one, making the directly grown MoS₂ conform to the rougher landscape of the transferred h-BN film underneath. The lower quality of the laser beam focus as well as the fluctuation of the domain surface could result in the decrease of the signal intensity for a confocal Raman apparatus.

Next, we investigated the photoluminescence (PL) of monolayer MoS₂ in different conditions. The PL spectra are normalized against the Raman intensity to show the relative luminescence quantum efficiency between different samples.²⁰ As depicted in Figure 4a, for the PL spectra of transferred MoS₂ on either h-BN or SiO₂ and the direct-grown MoS₂ on h-BN, which are proven to be almost strain-free in the lattice, there are mainly three subpeaks, located at ~ 625 , ~ 670 , and ~ 680 nm, respectively, which constitute the whole PL spectra of MoS₂. It is known that, for intrinsic monolayer MoS₂, two pronounced PL peaks located at ~ 670 nm (A peak) and ~ 625 nm (B peak) can be observed.^{27,20} The peak of A is due to the neutral exciton emission from the direct transition at the K point, and the B peak arises from exciton emission from another direct transition between the conduction band and a lower-lying valence band. However, the MoS₂ is easy to be unintentionally negatively doped when it is contaminated with some types of solvent or is just placed on SiO₂, which provides a relatively high level of trapped donors on the surface.^{33,39} Then, a third peak, located at lower energy than the A peak, emerges, and it can be associated with the recombination of negatively charged excitons of A (trions, A⁻), that is, a free electron bound to a neutral exciton *via* Coulomb interaction. Compared with the literature data, the observed three subpeaks in our PL for strainless MoS₂ correspond to the aforementioned B, A, and A⁻ excitonic transition modes, respectively.^{24,36,40,41} The energy difference between A and A⁻, which is ~ 30 meV, arises from the large binding energy of the second electron in A⁻.⁴⁰ We further extract quantitative information on three types of strainless MoS₂ by fitting the data to Lorentzian functions with three peaks located at wavelengths corresponding to B, A, and A⁻ excitonic species (Figure 4c–e). The results show a difference in integrated PL intensity ratio between A and A⁻ (A/A⁻), indicating that the relative populations of neutral to charged A excitons are affected by the doping level of MoS₂. The higher the doping level, the lower this ratio will be. It was found that the MoS₂ directly grown on h-BN has the highest A/A⁻, followed by transferred MoS₂ on h-BN, with

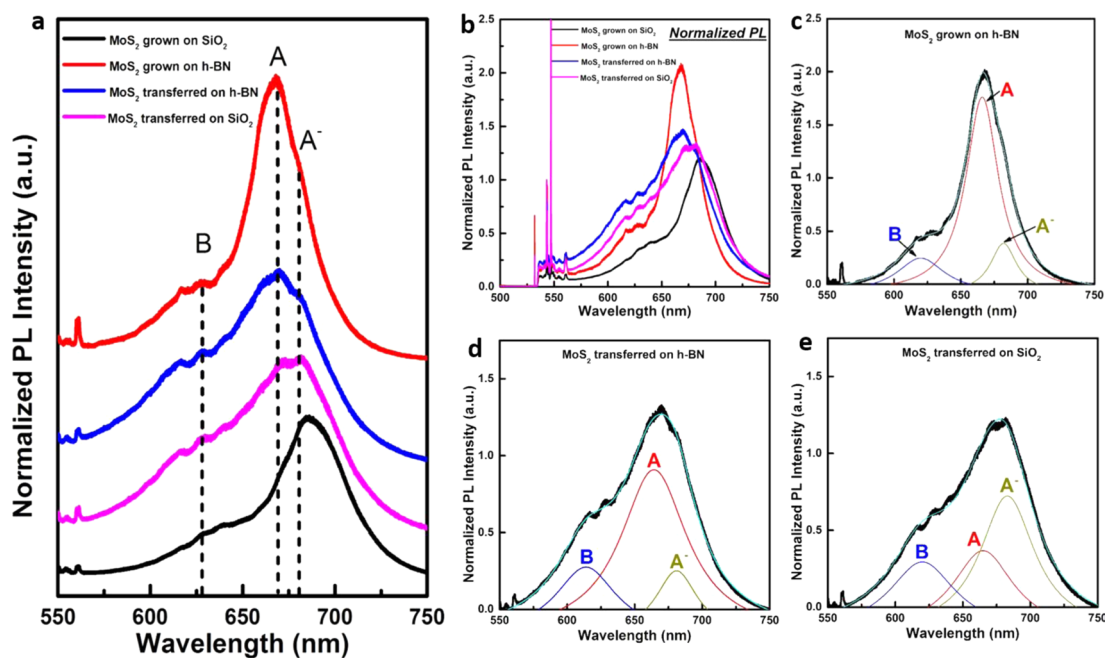


Figure 4. (a) PL spectra of the direct-grown and transferred MoS₂ on h-BN and SiO₂, respectively, which highlights the peak shape and location variation. The dashed black lines indicate the positions of three main peak emissions: B excitonic transition (B), the neutral excitonic transition of A (A), and the charged excitonic transition of A⁻ (A⁻), which can be easily found in the PL of strain-free MoS₂ domains, including the direct-grown MoS₂ on h-BN and the transferred MoS₂ on either h-BN or SiO₂. (b) PL spectra of the direct-grown and transferred MoS₂ on h-BN and on SiO₂, respectively, normalized by the MoS₂ Raman intensity to highlight the PL intensity variation. (c–e) Fits to the PL peak of strain-free MoS₂ with three subpeaks corresponding to A, A⁻, and B.

transferred MoS₂ on SiO₂ being the lowest. This observation further reveals the high degree of charged impurities for SiO₂, in agreement with the study of the Raman A_{1g} mode above and the contaminations introduced *via* a transfer process, which can also increase the doping level of MoS₂, making the transferred MoS₂ have a significantly lower A/A⁻ than the direct grown one even on the same substrate material of h-BN film. Moreover, in Figure 4a, for direct-grown MoS₂ on SiO₂, its PL peak corresponding to the direct transition at the K point experiences a red shift to ~686 nm, leading it to be in an even lower energy than the A⁻ transition mode of the strain-free MoS₂. We interpret the PL softening phenomenon as a signature of the tensile strain existence in the MoS₂ lattice, which is compatible with the analysis of the Raman E_{2g}¹ mode aforementioned and other recent studies because it has been reported that a uniaxial tensile strain can not only affect Raman modes but also reduce the band gap of monolayer MoS₂, leading to a red shift on its A excitonic transition mode.²⁷

As seen in Figure 4b, the direct-grown MoS₂ on h-BN has a stronger PL intensity with narrower fwhm (full width at half-maximum) than both transferred samples and direct-grown MoS₂ on SiO₂, indicating the higher crystallinity of the direct-grown MoS₂ on h-BN with a clean interface and a lower level of charged impurities. It is worth noting that the PL intensity of transferred MoS₂ on h-BN and on SiO₂ is similar, which means that

the substrate of h-BN does not show obvious advantage over SiO₂ when the contact between MoS₂ domains and substrates is realized through the transfer process instead of direct CVD growth. This could be due to the heavy doping effects on MoS₂ from solvent contaminations in the transfer, which covers up the superiority of the low charged impurity level of h-BN compared with SiO₂. This phenomenon further highlights the merits of using the CVD approach to fabricate such MoS₂/h-BN heterostructures.

CONCLUSIONS

In summary, we have demonstrated the fabrication of high-quality MoS₂/h-BN vertical van der Waals heterostructures through the direct CVD growth of monolayer MoS₂ on h-BN films. We utilized large-area h-BN films grown by CVD on copper, which are then transferred onto the SiO₂/Si substrates. Based on the analysis of Raman and PL spectra, we found that the direct CVD-grown MoS₂ crystals on the h-BN film suffered smaller lattice strain and lower doping levels than those directly grown on SiO₂. This led to a higher percentage of exciton recombination compared to trion recombination. In addition, this direct vapor-phase growth of MoS₂/h-BN heterostructures also had reduced contamination and better interlayer interactions at the interface, compared to those obtained *via* layer-by-layer polymer-assisted transfer methods. This direct and versatile fabrication approach of

MoS₂/h-BN heterostructures may have potential in electronic and optoelectronic applications and opens

up the possibility to create other types of TMD/h-BN heterostructures.

METHODS

CVD Growth of MoS₂/h-BN. The multilayer h-BN films were grown on copper foil (Cu, 25 μm, Alfa Aesar) with the precursor of ammonia borane (≥97%, Sigma-Aldrich) using atmospheric pressure CVD (APCVD). The growth was carried out at the temperature of 1000 °C for 40 min with argon and hydrogen mixed gas, while the ammonia borane powder was heated to ~80 °C. The as-grown multilayer h-BN films were then transferred onto the central area of a bare SiO₂/Si chip, which was subsequently used as the substrate to grow monolayer MoS₂. The synthesis of 2D MoS₂ occurred with the precursors of molybdenum trioxide (MoO₃, ≥99.5%, Sigma-Aldrich) and sulfur (S, ≥99.5%, Sigma-Aldrich) in APCVD using argon as the carrier gas. S powder was loaded in the outer 1 in. quartz tube at the central area of furnace 1, while MoO₃ was placed in the mini-tube at the upstream of furnace 2, being ~1–2 cm away from its left opening. The substrate was placed face-up in the center of furnace 2. After the system was flushed for 60 min with argon, S vapor was preintroduced into the growth region for 15 min by heating furnace 1 to 180 °C. Then the temperature of the second furnace was increased to ~800 °C at a speed of 40 °C/min and kept for 15 min under 150 sccm argon flow, and at the same time, the location where MoO₃ powder was placed reached a temperature of ~300 °C. Next, the argon flow rate was reduced to 10 sccm and maintained for 25 min, followed by a fast cooling process. More detailed CVD growth procedures for multilayer h-BN films and 2D MoS₂ on h-BN are provided in the Supporting Information.

Raman and PL Characterization. Raman and PL spectra, including corresponding mappings were measured using a JY Horiba LabRAM ARAMIS imaging confocal Raman microscope under a laser excitation wavelength of 532 nm with a power of ~2 mW at room temperature. The spot size of the laser was ~1 μm. For the measurement of MoS₂ spot spectra, the acquisition time was 2 s with the accumulation being twice that. For the measurement of Raman mapping, the acquisition time was 0.1 s for each spot with a step size of ~0.8 μm. When h-BN film was measured, the acquisition time was 30 s with the number of spectra averaged to be 1. The step size of the h-BN Raman map was ~1 μm.

Conflict of Interest: The authors declare no competing financial interest.

Acknowledgment. J.H.W. thanks the Royal Society for support. S.W. thanks the China Scholarship Council for support.

Supporting Information Available: More detailed CVD synthesis process of MoS₂/h-BN vertical heterostructures and characterizations of CVD-grown multilayer h-BN films, the coverage of 2D MoS₂ on h-BN, the calculation method of lattice strain in MoS₂ grown on SiO₂, discussion on the laser-induced thermal effects on Raman measurements, the phenomenon of various frequency differences between two characteristic monolayer MoS₂ Raman modes, and raw data of the Raman spectrum for 2D MoS₂ on the substrate of h-BN and SiO₂. This material is available free of charge via the Internet at <http://pubs.acs.org>.

REFERENCES AND NOTES

- Geim, A. K.; Grigorieva, I. V. van der Waals Heterostructures. *Nature* **2013**, *499*, 419–425.
- Britnell, L.; Gorbachev, R. V.; Jalil, R.; Belle, B. D.; Schedin, F.; Mishchenko, A.; Georgiou, T.; Katsnelson, M. I.; Eaves, L.; Morozov, S. V.; et al. Field-Effect Tunneling Transistor Based on Vertical Graphene Heterostructures. *Science* **2012**, *335*, 947–950.
- Georgiou, T.; Jalil, R.; Belle, B. D.; Britnell, L.; Gorbachev, R. V.; Morozov, S. V.; Kim, Y.-J.; Gholinia, A.; Haigh, S. J.; Makarovskiy, O.; et al. Vertical Field-Effect Transistor Based on Graphene-WS₂ Heterostructures for Flexible and Transparent Electronics. *Nat. Nanotechnol.* **2013**, *8*, 100–103.
- Yu, W. J.; Liu, Y.; Zhou, H.; Yin, A.; Li, Z.; Huang, Y.; Duan, X. Highly Efficient Gate-Tunable Photocurrent Generation in Vertical Heterostructures of Layered Materials. *Nat. Nanotechnol.* **2013**, *8*, 952–958.
- Cheng, R.; Li, D.; Zhou, H.; Wang, C.; Yin, A.; Jiang, S.; Liu, Y.; Chen, Y.; Huang, Y.; Duan, X. Electroluminescence and Photocurrent Generation from Atomically Sharp WSe₂/MoS₂ Heterojunction p-n Diodes. *Nano Lett.* **2014**, *14*, 5590–5597.
- Kretinin, A. V.; Cao, Y.; Tu, J. S.; Yu, G. L.; Jalil, R.; Novoselov, K. S.; Haigh, S. J.; Gholinia, A.; Mishchenko, A.; Lozada, M.; et al. Electronic Properties of Graphene Encapsulated with Different Two-Dimensional Atomic Crystals. *Nano Lett.* **2014**, *14*, 3270–3276.
- Haigh, S. J.; Gholinia, A.; Jalil, R.; Romani, S.; Britnell, L.; Elias, D. C.; Novoselov, K. S.; Ponomarenko, L. A.; Geim, A. K.; Gorbachev, R. Cross-Sectional Imaging of Individual Layers and Buried Interfaces of Graphene-Based Heterostructures and Superlattices. *Nat. Mater.* **2012**, *11*, 764–767.
- Gong, Y.; Lin, J.; Wang, X.; Shi, G.; Lei, S.; Lin, Z.; Zou, X.; Ye, G.; Vajtai, R.; Yakobson, B. I.; et al. Vertical and In-Plane Heterostructures from WS₂/MoS₂ Monolayers. *Nat. Mater.* **2014**, *13*, 1135–1142.
- Liu, Z.; Song, L.; Zhao, S.; Huang, J.; Ma, L.; Zhang, J.; Lou, J.; Ajayan, P. M. Direct Growth of Graphene/Hexagonal Boron Nitride Stacked Layers. *Nano Lett.* **2011**, *11*, 2032–2037.
- Shi, Y.; Zhou, W.; Lu, A.-Y.; Fang, W.; Lee, Y.-H.; Hsu, A. L.; Kim, S. M.; Kim, K. K.; Yang, H. Y.; Li, L.-J.; et al. van der Waals Epitaxy of MoS₂ Layers Using Graphene as Growth Templates. *Nano Lett.* **2012**, *12*, 2784–2791.
- Shim, G. W.; Yoo, K.; Seo, S.-B.; Shin, J.; Jung, D. Y.; Kang, I.-S.; Ahn, C. W.; Cho, B. J.; Choi, S.-Y. Large-Area Single-Layer MoSe₂ and Its van der Waals Heterostructures. *ACS Nano* **2014**, *8*, 6655–6662.
- Ling, X.; Lee, Y.; Lin, Y.; Fang, W.; Yu, L.; Dresselhaus, M. S.; Kong, J. Role of the Seeding Promoter in MoS₂ Growth by Chemical Vapor Deposition. *Nano Lett.* **2014**, *14*, 464–472.
- Okada, M.; Sawazaki, T.; Watanabe, K.; Taniguchi, T.; Hibino, H.; Shinohara, H.; Kitaura, R. Direct Chemical Vapor Deposition Growth of WS₂ Atomic Layers on Hexagonal Boron Nitride. *ACS Nano* **2014**, *8*, 8273–8277.
- Zhang, X.; Meng, F.; Christianson, J. R.; Arroyo-Torres, C.; Lukowski, M. A.; Liang, D.; Schmidt, J. R.; Jin, S. Vertical Heterostructures of Layered Metal Chalcogenides by van der Waals Epitaxy. *Nano Lett.* **2014**, *14*, 3047–3054.
- Dean, C. R.; Young, A. F.; Meric, I.; Lee, C.; Wang, L.; Sorgenfrei, S.; Watanabe, K.; Taniguchi, T.; Kim, P.; Shepard, K. L.; et al. Boron Nitride Substrates for High-Quality Graphene Electronics. *Nat. Nanotechnol.* **2010**, *5*, 722–726.
- Gannett, W.; Regan, W.; Watanabe, K.; Taniguchi, T.; Crommie, M. F.; Zettl, A. Boron Nitride Substrates for High Mobility Chemical Vapor Deposited Graphene. *Appl. Phys. Lett.* **2011**, *98*, 242105.
- Zhang, J.; Yu, H.; Chen, W.; Tian, X.; Liu, D.; Cheng, M.; Xie, G.; Yang, W.; Yang, R.; Bai, X.; et al. Scalable Growth of High-Quality Polycrystalline MoS₂ Monolayers on SiO₂ with Tunable Grain Sizes. *ACS Nano* **2014**, *8*, 6024–6030.
- Gorbachev, R. V.; Riaz, I.; Nair, R. R.; Jalil, R.; Britnell, L.; Belle, B. D.; Hill, E. W.; Novoselov, K. S.; Watanabe, K.; Taniguchi, T.; et al. Hunting for Monolayer Boron Nitride: Optical and Raman Signatures. *Small* **2011**, *7*, 465–468.
- Wang, S.; Rong, Y.; Fan, Y.; Pacios, M.; Bhaskaran, H.; He, K.; Warner, J. H. Shape Evolution of Monolayer MoS₂ Crystals Grown by Chemical Vapor Deposition. *Chem. Mater.* **2014**, *26*, 6371–6379.

20. Splendiani, A.; Sun, L.; Zhang, Y.; Li, T.; Kim, J.; Chim, C.-Y.; Galli, G.; Wang, F. Emerging Photoluminescence in Monolayer MoS₂. *Nano Lett.* **2010**, *10*, 1271–1275.
21. Tonndorf, P.; Schmidt, R.; Böttger, P.; Zhang, X.; Börner, J.; Liebig, A.; Albrecht, M.; Kloc, C.; Gordan, O.; Zahn, D. R. T.; et al. Photoluminescence Emission and Raman Response of Monolayer MoS₂, MoSe₂ and WSe₂. *Opt. Express* **2013**, *21*, 4908–4916.
22. Najmaei, S.; Liu, Z.; Zhou, W.; Zou, X.; Shi, G.; Lei, S.; Yakobson, B. I.; Idrobo, J.-C.; Ajayan, P. M.; Lou, J. Vapour Phase Growth and Grain Boundary Structure of Molybdenum Disulphide Atomic Layers. *Nat. Mater.* **2013**, *12*, 754–759.
23. Wang, X.; Feng, H.; Wu, Y.; Jiao, L. Controlled Synthesis of Highly Crystalline MoS₂ Flakes by Chemical Vapor Deposition. *J. Am. Chem. Soc.* **2013**, *135*, 5304–5307.
24. Buscema, M.; Steele, G. A.; van der Zant, H. S. J.; Castellanos-Gomez, A. The Effect of the Substrate on the Raman and Photoluminescence Emission of Single-Layer MoS₂. *Nano Res.* **2014**, *7*, 1–11.
25. Liu, K.; Yan, Q.; Chen, M.; Fan, W.; Sun, Y.; Suh, J.; Fu, D.; Lee, S.; Zhou, J.; Tongay, S.; et al. Elastic Properties of Chemical-Vapor-Deposited Monolayer MoS₂, WS₂, and Their Bilayer Heterostructures. *Nano Lett.* **2014**, *14*, 5097–5103.
26. Zhou, K.; Withers, F.; Cao, Y.; Hu, S.; Yu, G.; Casiraghi, C. Raman Modes of MoS₂ Used as Fingerprint of van der Waals Interactions. *ACS Nano* **2014**, *8*, 9914–9924.
27. Conley, H. J.; Wang, B.; Ziegler, J. I.; Haglund, R. F.; Pantelides, S. T.; Bolotin, K. I. Bandgap Engineering of Strained Monolayer and Bilayer MoS₂. *Nano Lett.* **2013**, *13*, 3626–3630.
28. Rice, C.; Young, R.; Zan, R.; Bangert, U.; Wolverson, D.; Georgiou, T.; Jalil, R.; Novoselov, K. Raman-Scattering Measurements and First-Principles Calculations of Strain-Induced Phonon Shifts in Monolayer MoS₂. *Phys. Rev. B* **2013**, *87*, 081307.
29. Hui, Y. Y.; Liu, X.; Jie, W.; Chan, N. Y.; Hao, J.; Hsu, Y.-T.; Li, L.-J.; Guo, W.; Lau, S. P. Exceptional Tunability of Band Energy in a Compressively Strained Trilayer MoS₂ Sheet. *ACS Nano* **2013**, *7*, 7126–7131.
30. Yang, L.; Cui, X.; Zhang, J.; Wang, K.; Shen, M.; Zeng, S.; Dayeh, S. A.; Feng, L.; Xiang, B. Lattice Strain Effects on the Optical Properties of MoS₂ Nanosheets. *Sci. Rep.* **2014**, *4*, 5649.
31. Cai, Y.; Lan, J.; Zhang, G.; Zhang, Y.-W. Lattice Vibrational Modes and Phonon Thermal Conductivity of Monolayer MoS₂. *Phys. Rev. B* **2014**, *89*, 035438.
32. Chakraborty, B.; Bera, A.; Muthu, D. V. S.; Bhowmick, S.; Waghmare, U. V.; Sood, A. K. Symmetry-Dependent Phonon Renormalization in Monolayer MoS₂ Transistor. *Phys. Rev. B* **2012**, *85*, 161403.
33. Mao, N.; Chen, Y.; Liu, D.; Zhang, J.; Xie, L. Solvatochromic Effect on the Photoluminescence of MoS₂ Monolayers. *Small* **2013**, *9*, 1312–1315.
34. Bao, W.; Cai, X.; Kim, D.; Sridhara, K.; Fuhrer, M. S. High Mobility Ambipolar MoS₂ Field-Effect Transistors: Substrate and Dielectric Effects. *Appl. Phys. Lett.* **2013**, *102*, 042104.
35. Mos, T.; Ghatak, S.; Pal, A. N.; Ghosh, A. Nature of Electronic States in Atomically Thin MoS₂ Field-Effect Transistors. *ACS Nano* **2011**, *5*, 7707–7712.
36. Tongay, S.; Zhou, J.; Ataca, C.; Liu, J.; Kang, J. S.; Matthews, T. S.; You, L.; Li, J.; Grossman, J. C.; Wu, J. Broad-Range Modulation of Light Emission in Two-Dimensional Semiconductors by Molecular Physisorption Gating. *Nano Lett.* **2013**, *13*, 2831–2836.
37. Sahoo, S.; Gaur, A. P. S.; Ahmadi, M.; Katiyar, R. S. Temperature-Dependent Raman Studies and Thermal Conductivity of Few-Layer MoS₂. *J. Phys. Chem. C* **2013**, *117*, 9042–9047.
38. Najmaei, S.; Liu, Z.; Ajayan, P. M.; Lou, J. Thermal Effects on the Characteristic Raman Spectrum of Molybdenum Disulfide (MoS₂) of Varying Thicknesses. *Appl. Phys. Lett.* **2012**, *100*, 013106.
39. Lu, C.; Li, G.; Mao, J.; Wang, L.; Andrei, E. Y. Bandgap, Mid-Gap States, and Gating Effects in MoS₂. *Nano Lett.* **2014**, *14*, 4628–4633.
40. Mak, K. F.; He, K.; Lee, C.; Lee, G. H.; Hone, J.; Heinz, T. F.; Shan, J. Tightly Bound Trions in Monolayer MoS₂. *Nat. Mater.* **2013**, *12*, 207–211.
41. Ross, J. S.; Wu, S.; Yu, H.; Ghimire, N. J.; Jones, A. M.; Aivazian, G.; Yan, J.; Mandrus, D. G.; Xiao, D.; Yao, W.; et al. Electrical Control of Neutral and Charged Excitons in a Monolayer Semiconductor. *Nat. Commun.* **2013**, *4*, 1474.